J. Fluid Mech. (1971), *vol.* 45, *part* 3, *pp.* 417–440
Printed in Great Britain

An elastic sublayer model for drag reduction by dilute solutions of linear macromolecules

By P. S. VIRK

Department of Chemical Engineering
Massachusetts Institute of Technology

(Received 1 April 1970)

Further evidence of a universal maximum drag reduction asymptote is presented. In the elastic sublayer model, inferred therefrom, the mean velocity profile during drag reduction is approximated by three zones: the usual viscous sublayer, an elastic sublayer where the mixing-length constant is derived from the maximum drag reduction asymptote, and an outermost region with Newtonian mixing-length constant. Upon integration the model yields a friction factor relation, parametric in elastic sublayer thickness, which properly reproduces the known features of turbulent dilute polymer solution flow. The dependence of elastic sublayer thickness upon flow and polymeric parameters is inferred from experimental data revealing two hitherto unknown relationships: namely that on Prandtl co-ordinates, $1/f^{\frac{1}{2}}$ *vs.* log $Ref^{\frac{1}{2}}$, the difference in slope between a polymer solution and solvent is proportional to the square root of molar concentration and to the three-halves power of backbone chain links in the macromolecule. The proportionality constant in the preceding relationship is approximately the same for several different polymer species of carbon-carbon or similar skeletal structure in various thin solvents; there is an indication that this constant further depends upon the product of solvent viscosity times the cube of the effective bond length per chain link of the polymer species. Some recent results regarding the onset of drag reduction are also summarized.

1. Introduction

Toms phenomenon (Toms 1948), drag reduction by dilute polymer solutions in turbulent pipe flow, has thus far been studied experimentally in three echelons of increasing detail: pressure drop versus flow rate or gross flow measurements, mean velocity profiles and turbulence structure measurements. Gross flow studies (e.g. Savins 1964; Elata & Tirosh 1965; Virk *et al.* 1967; Hershey & Zakin 1967; Liaw 1968) indicate the existence of three régimes of turbulent flow, in order of increasing flow rate: (i) A régime without drag reduction wherein the polymer solutions obey the same friction factor relation as solvent. (ii) A régime with drag reduction in which the friction factor relation obeyed by a given solution depends upon all identifiable polymeric parameters—the polymer-solvent system, polymer molecular weight and concentration. The demarcation between régimes (i) and (ii), i.e. the onset of drag reduction, is usually quite well defined. (iii) An asymptotic régime which ultimately limits the maximum drag reduction possible

in Toms phenomenon. The friction factor relation for this ultimate asymptote is independent of polymeric parameters. Of the mean velocity profiles reported to date (Elata, Lehrer & Kahanovitz 1966; Virk *et al.* 1967; Goren & Norbury 1967; Wells, Harkness & Meyer 1968; Patterson & Florez 1969; Seyer & Metzner 1969), most have been measured at conditions of relatively low drag reduction in the 'polymeric' régime (ii) above. On U^+ *vs.* y^+ co-ordinates, these polymer solution profiles exhibit a characteristic shift upward from but parallel to the semi-logarithmic Newtonian law of the wall over that portion of the pipe radius, the outer flow, where the latter applies. The structure of turbulence during drag reduction has been studied to the extent of a few turbulent intensity profiles and kinetic energy spectra (Virk *et al.* 1967; Wells *et al.* 1968; Spangler 1969; Seyer & Metzner 1969) but the results are, as yet, inconclusive.

From a theoretical standpoint the mechanism of drag reduction is still obscure but two significant impressions appear to have emerged. First, that the phenomenon stems from some kind of a time domain interaction between the polymeric solute and the turbulent flow field and, secondly, that the polymer-turbulence interaction, however it occurs, most significantly affects the region very close to the bounding wall. Concerning the former, an association of drag reduction with 'visco-elasticity' dates to some early papers on the subject (Savins 1964; Metzner & Park 1964; Wells 1965) but probably the most plausible physical connexion, in terms of macromolecular strain energy, is due to Walsh (1967). The experimental support for this is provided, albeit indirectly, by the observation that at the onset of drag reduction the reciprocal wall shear rate, a time-scale characteristic of the wall turbulence, is of the order of magnitude of the terminal relaxation time of the macromolecule (Elata, Lehrer & Kahanovitz 1966; Fabula, Lumley & Taylor 1966; Hershey & Zakin 1967) as calculated from linear visco-elasticity theory (Rouse 1953; Zimm 1956) even though the size of the macromolecule is much smaller than, of order 10^{-3} times, that of the typical dissipative eddy (Virk *et al.* 1967). The relevance of the wall region, first anticipated by Oldroyd (1948) and almost universally accepted since, is supported and clarified by two kinds of experimental evidence. Mean velocity profiles at low drag reduction indicate that the region affected by the macromolecules lies closer to the wall than the inner edge $y^+ \sim 50$ of the outer flow. Recent data in rough pipes (McNally 1968; Spangler 1969; Virk 1971) show that the onset of drag reduction is virtually unaffected by the presence (hydraulically smooth flow) or absence (fully rough flow) of a viscous sublayer which suggests that the polymer-turbulence interaction starts further from the wall than $y^+ \sim 5$. Together, these imply that the buffer zone $5 < y^+ < 50$, of known importance (Laufer 1954) in the energetics of turbulent Newtonian pipe flow, is where the processes responsible for drag reduction commence. The same qualitative result has also been inferred from theoretical arguments concerning possible changes in wall region energy spectra during drag reduction (Lumley 1967, 1969).

Despite the aforementioned advances there is still no satisfactory description of the numerous variables which influence drag reduction and the purpose of this paper is to present an approximate, physically motivated, mean flow model for Toms phenomenon from which the dependence of drag reduction upon flow

and polymeric parameters can be ascertained. The model is based on a three-zone scheme for the mean velocity profile (Virk, Mickley & Smith 1970) in which drag reduction was associated with an 'interactive zone' or 'elastic sublayer' juxtaposed between a viscous sublayer and a Newtonian outer flow. In the present work the previous mean velocity profile is integrated to yield a general friction factor relation that is parametric in the thickness of the elastic sublayer. Elastic sublayer thickness is then related to macromolecular parameters (concentration, molecular weight and backbone chain links) by inference from experimental measurements. The empirical relations so obtained are partially interpreted and somewhat extended by a brief theoretical analysis of the polymer-turbulence interaction. Finally, the model devised is compared with previous schemes (Oldroyd 1948; Elata *et al.* 1966; Meyer 1966; Seyer & Metzner 1969) and some points concerning its practical application are noted.

2. The elastic sublayer model

2.1. *Asymptotic friction factor relations*

In friction factor co-ordinates, the region of Toms phenomenon is bounded by asymptotes of zero and maximum drag reduction, both independent of polymeric parameters, and any general mean flow model must reduce to these asymptotes at the appropriate extremes. The zero drag reduction asymptote is, of course, the well known Prandtl–von Kármán law for Newtonian turbulent pipe flow.

$$1/f^{\frac{1}{2}} = 4{\cdot}0\log_{10}(Ref^{\frac{1}{2}}) - 0{\cdot}4, \tag{1}$$

where f and Re are the usual Fanning friction factor and diametral Reynolds number respectively. The maximum drag reduction asymptote, first reported by the present author (Virk *et al.* 1967), has since been observed in several independent studies the results of which are correlated (Virk *et al.* 1970) by

$$1/f^{\frac{1}{2}} = 19{\cdot}0\log_{10}(Ref^{\frac{1}{2}}) - 32{\cdot}4. \tag{2}$$

The correlation (2) was based mainly on data for aqueous polyethyleneoxide solutions but in the interim since its development maximum drag reduction data have been reported in pipe flow with numerous different polymers dissolved in aqueous and in organic solvents (Liaw 1968; Whittsitt, Harrington & Crawford 1968; Virk & Baher 1970; Virk 1971). Moreover, the above dilute polymer solution asymptote also appears to limit the maximum drag reduction achieved with complex soap solutions (White 1967). This further evidence of a universal maximum drag reduction asymptote is illustrated in figure 1, a friction factor plot with Prandtl co-ordinates $1/f^{\frac{1}{2}}$ *vs.* log $(Ref^{\frac{1}{2}})$; corresponding experimental details are given in table 1. The more recent data can be seen to agree well with the solid line representing the earlier correlation. It is also worth noting that the pipe flow relation (2) permits the inference of corresponding asymptotes in external flow configurations (Virk *et al.* 1970) and there are the most preliminary indications that such asymptotes occur in turbulent boundary-layer flow past a flat plate (Fruman & Sulmont 1968) and on a free spinning disk (Hoyt & Fabula 1964; Gilbert & Ripken 1969).

2.2. *The three zone mean velocity profile*

Mean velocity profiles prevailing under asymptotic conditions can be inferred from the corresponding friction factor relations. Transformation of the correlation (2) yields the mean velocity profile

$$U^+ = 11{\cdot}7 \ln y^+ - 17{\cdot}0, \tag{3}$$

ultimately attained at maximum drag reduction. This ultimate profile is noteworthy in that it shares a tri-section, at $(U^+, y^+) = (11{\cdot}6, 11{\cdot}6)$, with the usual viscous sublayer

$$U^+ = y^+ \tag{4}$$

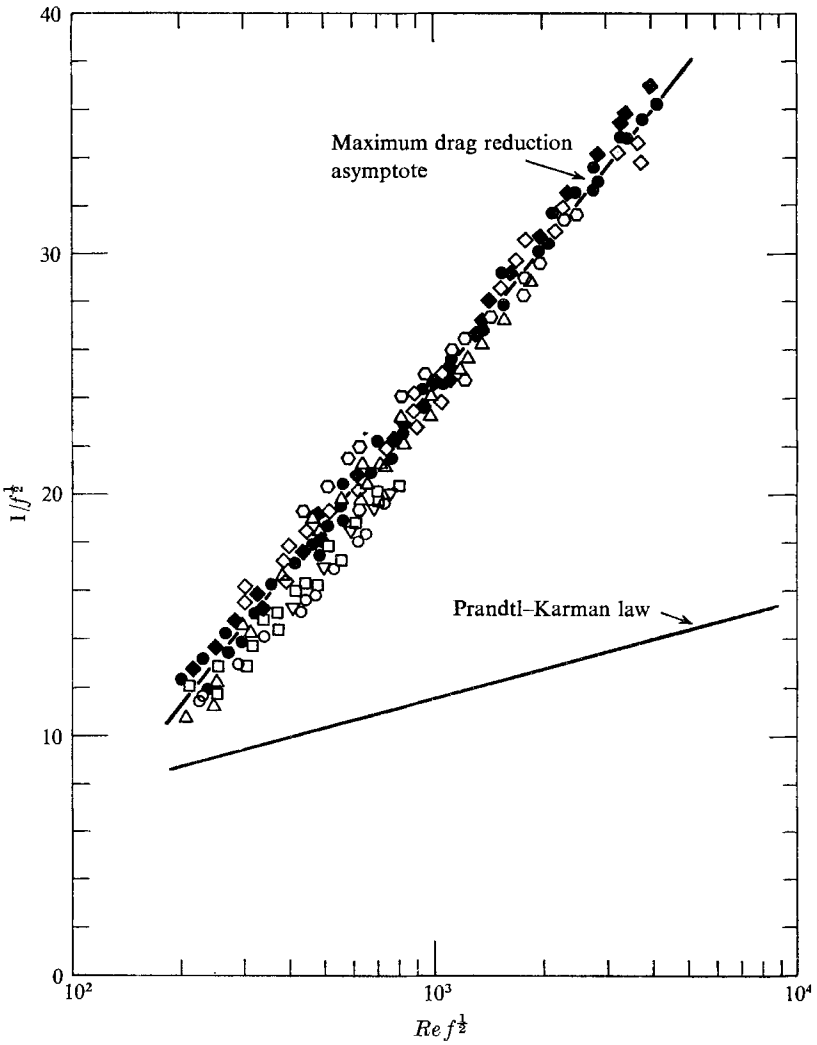

FIGURE 1. Further evidence of a maximum drag reduction asymptote in pipe flow. Symbols are numbered to correspond to entries in table 1. ⟨⟩, 1; ◇, 2; ◆, 3; ●, 4; ○, 5; □, 6; ▽, 7; △, 8.

Entry	Source	Solvent	Polymer	M $\times 10^{-6}$	c w.p.p.m.	Pipe I.D. (cm)
1	Whittsitt *et al.* (1968)	Water	GGM	(0·22)	1250	0·457, 1·06
2		Water	PAMH	(3)	250	0·457, 1·06
3	Virk & Baher (1970)	Water	PAM	4·7	300, 1000	0·953
	Virk (1971)			12·5	40, 100	0·846
4		Water	PEO	5·5	30, 100	0·846
				8·0	100	0·846
5	Liaw (1968)	Benzene	PEO	3·1	80, 200	0·083, 0·166, 0·272
6		Toluene	PDMS	10·7	30	0·083, 0·166, 0·272
				5·6	500	0·083, 0·166, 0·272
7		Toluene	PCIP	2·2	200	0·083
8	White (1967)	Water	CTAB-Naphthol (complex soap)		500	0·228, 0·635, 1·27, 1·41, 3·81

Notes

Entries are ordered to correspond with legend of figure 1.

CTAB-Naphthol. Equimolar Cetyltrimethyl-ammonium-bromide and 1-Naphthol.

Numbers in parentheses are estimated, not experimental.

TABLE 1. Summary of recent maximum drag reduction data

Polymer notation

Species		m	b
GGM	Guar gum	243	20
PAM	Polyacrylamide, homopolymer	35·5	5.2
PAMH	Polyacrylamide, hydrolysed	(35·5)	5·2
PCIP	Polycisisoprene	22·7	3·8
PDMS	Polydimethylsiloxane	30	3·9
PEO	Polyethyleneoxide	14·7	3.2
PIB	Polyisobutylene	28	3·9
PMMA	Polymethylmethacrylate	50	4·5

m molecular weight per backbone chain link.

b effective bond length (unperturbed) Å.
Values are from Kurata & Stockmayer (1963) except for GGM (after Koleske & Kurath 1964) and PEO (Beech & Booth 1969).

$[\eta]$ intrinsic viscosity in decilitres/gram.

M weight average molecular weight.

N number of backbone chain links per molecule.

Π intrinsic slope increment defined by equation (17).

and Newtonian law of the wall

$$U^+ = 2{\cdot}5 \ln y^+ + 5{\cdot}5, \tag{5}$$

of which (5) is related to (1) as (3) is to (2). Figure 2, $U^+ vs. \log y^+$, shows experimental mean velocity profiles obtained during drag reduction (Elata *et al.* 1966; Virk *et al.* 1967; Goren & Norbury 1967; Patterson & Florez 1969; Seyer & Metzner 1969). The latter two sets of data, unavailable at the time of the earlier

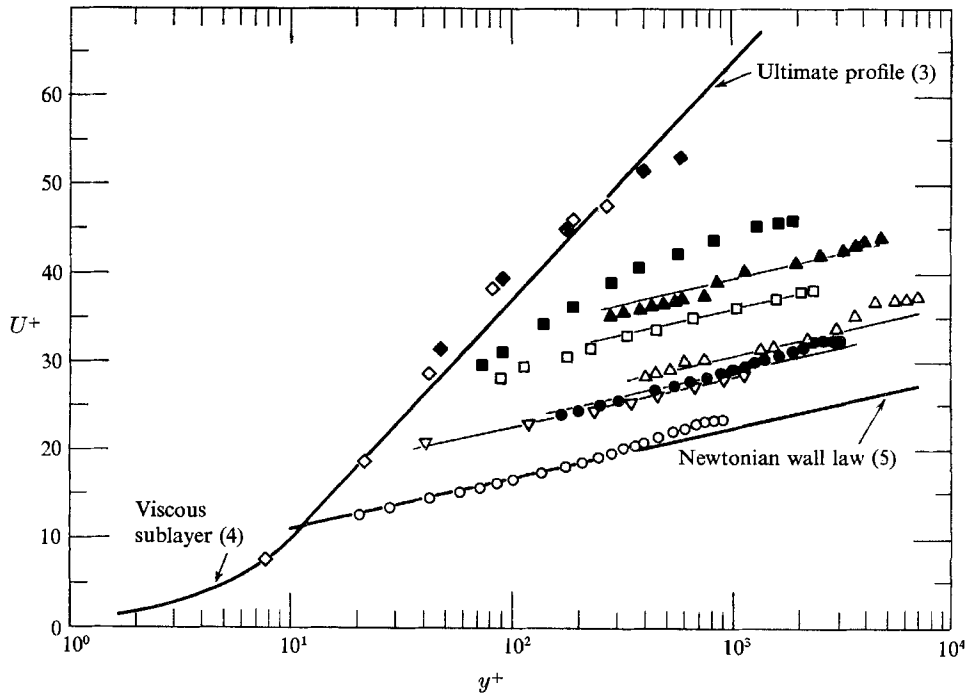

FIGURE 2. Experimental mean velocity profiles during drag reduction. Numbered lines correspond to equations in text. Symbols are numbered to correspond to entries in table 2. △, 1; ▲, 2; □, 3; ■, 4; ▽, 5; ◇, 6; ◆, 7; ○, 8; ●, 9.

work from which the figure is adapted, are each separately noteworthy; Patterson's profiles are amongst the first such in organic solvents while Seyer's data represent the only available results at (or near) maximum drag reduction. From figure 2 it is evident that the experimental profiles are bounded by the asymptotic profiles (5) and (3). At intermediate but low drag reductions the data show the parallel upshift relative to solvent (5); as drag reduction increases there is a tendency towards the ultimate profile (3). Based on this purely experimental evidence it is reasonable to suppose that in the general case of drag reduction the mean velocity profile consists of three segments, which are, proceeding from pipe wall to pipe axis, (1) a viscous sublayer, akin to Newtonian; (2) an interactive zone, characteristic of drag reduction; (3) an outer region, 'Newtonian plug', with Newtonian mixing-length constant. The main feature of this scheme is the interactive zone, here renamed the *elastic sublayer*, associated with drag reduction and because the

maximum drag reduction asymptote appears to be universal the mean velocity profile in the elastic sublayer is assumed always to be a segment of the ultimate profile (3). The extent of drag reduction then depends solely upon the location of the outer edge of the elastic sublayer, y_e^+, inasmuch as the interface, y_v^+, between the viscous and elastic sublayers is uniquely defined by the trisection of

Entry	Source	Solvent	Polymer	M $\times 10^{-6}$	c w.p.p.m.	Pipe I.D. (cm)	$Ref^{\frac{1}{2}}$	$1/f^{\frac{1}{2}}$	S_F
1	Elata *et al.* (1966)	Water	GGM	(0·5)	400	5·07	20,500	22·3	0·32
2					800		14,500	28·2	0·74
3	Goren & Norbury (1967)	Water	PEO	(5)	2·5	5·08	6,200	24·2	0·64
4					10		5,300	28·2	0·94
5	Patterson & Florez (1969)	Cyclo-hexane	PIB	0·5	2,000	2·54	3,200	17·3	0·27
6	Seyer & Metzner (1969)	Water	PAMH	(3)	1,000	2·54	780	23·2	1·02
7					1,000		1,680	29·2	1·34
8	Virk *et al.* (1967)	Water	PEO	0·69	1,000	3·21	2,700	13·5	0
9					1,000		8,950	19·9	0·29

Notes

Entries are ordered to correspond with legend of figure 2.

Polymer abbreviations as noted below table 1.

Molecular weights in parentheses are order of magnitude estimates only since no data given in original.

$S_F = [(f_s/f_p)^{\frac{1}{2}} - 1]_{Ref^{\frac{1}{2}}}$ is the fractional slip, a measure of drag reduction, defined as the fractional increase of $1/f^{\frac{1}{2}}$ with polymer solution relative to Newtonian at the same $Ref^{\frac{1}{2}}$ in the given pipe.

TABLE 2. Summary of mean velocity profile data

equations (3), (4), and (5). As drag reduction is decreased, $y_e^+ \to y_v^+$ and the model tends to the Taylor–Prandtl Newtonian scheme; as drag reduction is increased, $y_e^+ \to R^+$ and the ultimate profile tends to prevail over the entire cross-section. At intermediate drag reductions the profile displays an 'effective slip', incurred across the elastic sublayer, whereby the outer, Newtonian plug, region is parallel-shifted upward relative to solvent (5). The model thus reduces to the proper limiting cases at zero and maximum drag reduction and, between these limits, is consistent with all available experimental observations.

The utility of the above, highly idealized, scheme clearly hinges upon a viable description of elastic sublayer extent. To this end, the model is next integrated to provide a general friction factor relationship in terms of y_e^+; a relationship between y_e^+ and the macromolecular and flow parameters affecting drag reduction is then inferred from experiments.

2.3. *Integration for friction factor*

The non-dimensional velocity profile, U^+ (y^+), for the model outlined possesses three segments

$$U^+ = y^+ : 0 \leqslant y^+ \leqslant y_v^+, \tag{6a}$$

$$U^+ = A_2 \ln y^+ + B_2 : y_v^+ \leqslant y^+ \leqslant y_e^+, \tag{6b}$$

$$U^+ = A_3 \ln y^+ + B_3 : y_e^+ \leqslant y^+ \leqslant R^+. \tag{6c}$$

In the above, $U^+ = (U/u_\tau)$ and $y^+ = (yu_\tau/\nu)$ are the usual law of the wall parameters, U being the mean axial velocity at distance y from the pipe wall; u_τ is friction velocity and ν kinematic viscosity. Numerical subscripts 1, 2, 3 refer respectively to the viscous sublayer, elastic sublayer and Newtonian plug; subscript v refers to the interface between zones 1 and 2 while subscript e refers to the interface between zones 2 and 3. R^+ is the value of y^+ on the pipe axis. A and B are the constants associated with a semi-logarithmic segment and to stress their universality, A_2, B_2 are renamed A_m, B_m (subscript m to signify an association with the maximum drag reduction asymptote) and A_3 renamed A_n (subscript n for Newtonian). Appropriate current numerical values are $(A_m, B_m) = (11{\cdot}7, -17{\cdot}0)$ and $(A_n, B_n) = (2{\cdot}5, 5{\cdot}5)$, the slopes (A_m, A_n) being the reciprocals, respectively, of the ultimate and Newtonian mixing-length constants, $(X_m, X_n) = (0{\cdot}085, 0{\cdot}40)$. Note that B_3 is defined by the intersection of $(6b)$ and $(6c)$ at y_e^+ so that

$$B_3 = B_n + (A_m - A_n)\ln(y_e^+/y_v^+). \tag{7}$$

By definition, the average velocity U_{av} across the pipe cross-section is

$$U_{\mathrm{av}} = \frac{Q}{\pi R^2} = \int_0^1 U d(1-\xi)^2, \tag{8}$$

where Q is the volumetric flow rate and $\xi = (y/R)$ the radius-normalized distance from the pipe wall. In terms of the friction factor, with the integral on the right-hand side of (8) decomposed by segments using $(6a, b, c)$,

$$\frac{U_{\mathrm{av}}}{u_\tau} = U_{\mathrm{av}}^+ = 2\left[\int_0^{\xi_v} U_1^+(1-\xi)d\xi + \int_{\xi_v}^{\xi_e} U_2^+(1-\xi)d\xi + \int_{\xi_e}^1 U_3^+(1-\xi)d\xi\right]. \tag{9}$$

All three integrals on the right-hand side of (9) can readily be evaluated. The first integral, i.e. the viscous sublayer, contributes a fractional amount $(2y_v^{+2}/Re) \ll 1$ to U_{av}^+ and therefore little error is incurred by taking $\xi_v \sim 0$ for analytical simplicity. The latter two integrals on the right-hand side of (9) are of an identical form and applying the proper limits, collecting terms and substituting the relevant constants one obtains

$$U_{\mathrm{av}}^+ = A_n \ln R^+ + B_n - \tfrac{3}{2}A_n + (A_m - A_n)[\ln(\xi_e R^+) - 2\xi_e(1 - \tfrac{1}{4}\xi_e)] + B_m - B_n. \tag{10}$$

Equation (10) is the basic friction factor relation resulting from our mean flow model, expressed in terms of the outer edge ξ_e, of the elastic sublayer. It is readily shown that (10) transforms to the appropriate asymptotes:

$$U_{\mathrm{av}}^+ = A_n \ln R^+ + B_n - \tfrac{3}{2}A_n, \quad \xi_e \to 0; \tag{11a}$$

$$U_{\mathrm{av}}^+ = A_m \ln R^+ + B_m - \tfrac{3}{2}A_m, \quad \xi_e \to 1; \tag{11b}$$

where $\xi \to 0$ is taken to mean $y_e^+ \to y_v^+$. Between the limits $0 < \xi_e < 1$ the friction factor, and hence drag reduction, depend upon ξ_e through the square bracket on the right-hand side of (10). Of the two terms therein the logarithmic term dominates, as shown in table 3, and if $2\xi_e(1 - \frac{1}{4}\xi_e)$ is neglected in comparison with $\ln(\xi_e R^+)$ the general friction factor relation simplifies to:

$$U_{\mathrm{av}}^+ = A_n \ln R^+ + B_n - \tfrac{3}{2}A_n + (A_m - A_n)\ln(y_e^+/y_v^+), \quad y_v^+ < y_e^+ < R^+. \tag{12}$$

2.4. *Relation to polymeric parameters*

A relationship between elastic sublayer thickness, y_e^+, and the flow and polymeric parameters affecting drag reduction is suggested by two experimental observations valid for dilute solutions of linear, random-coiling macromolecules in the polymeric régime. First, for a given polymer and solvent, the onset of drag reduction occurs essentially independent of polymer concentration and

R^+ →	100	300	1000	3000	10,000
ξ_e ↓	—	—	—	—	—
0·01	—	—	0·008	0·005	0·004
0·03	—	0·027	0·017	0·013	0·010
0·10	0·084	0·057	0·042	0·034	0·028
0·30	0·163	0·123	0·097	0·059	0·049
1·00	0·325	0·262	0·217	0·187	0·162

TABLE 3. Selected values of $[2\xi_e(1-\frac{1}{4}\xi_e)/\ln(\xi_e R^+)]$

second, following onset, the polymer solutions describe approximately straight lines in Prandtl co-ordinates, $U_{\mathrm{av}}^+ vs. \ln R^+$, with slopes increasing progressively with concentration. Physically these indicate that two kinds of factors influence drag reduction; those, reflected by onset and the affine straight line behaviour thereafter, which are independent of concentration and can be associated with the 'excitation' of an individual macromolecule by the turbulent flow field and those, reflected by the slopes, which appear related to the 'amount' of polymer present. A function for elastic sublayer thickness that contains these two factors in separable form and applies for all R^+ is

$$\ln(y_e^+/y_v^+) = 0, \quad (R^+/R^{+*}) < 1; \tag{13a}$$

$$= \psi \ln(R^+/R^{+*}); \tag{13b}$$

$$= \ln(R^+/y_v^+), \quad (R^+/R^{+*}) > (R^{+*}/y_v^+)^{1/\psi-1}. \tag{13c}$$

In equation (13*b*), the operational member of the set, the entity ψ represents the 'amount' factor, which, by hypothesis, must depend solely on the molecular description of a polymer solution. The $\ln(R^+/R^{+*})$ term, where R^{+*} is the value of R^+ at the onset of drag reduction, describes the 'excitation' factor which depends both upon flow parameters and such polymeric parameters as are associated with the excitation of a macromolecule. Substitution of equations (13) into the general friction factor relation (10) readily demonstrates that the elastic sublayer function devised yields, in idealized form, all of the gross flow régimes observed in Toms phenomenon: (13*a*) results in the Newtonian friction factor asymptote (11*a*) and hence no drag reduction prior to onset; (13*b*) yields the polymeric régime with the characteristics noted above; while (13*c*), invoked for $\psi > 1$, results in the maximum drag reduction asymptote (11*b*). Focusing on the polymeric régime and substituting (13*b*) into the simplified friction factor relation (12) therein one obtains

$$U_{\mathrm{av}}^+ = (A_n + \delta)\ln R^+ + B_n - \tfrac{3}{2}A_n - \delta \ln R^{+*}, \tag{14}$$

where, by definition $$\delta = (A_m - A_n)\psi. \tag{15}$$

The slope increment δ, which is the same as the purely molecular entity ψ save for the constant, and universal, multiplier $(A_m - A_n)$, is the difference between the slopes of polymer solution and solvent friction factor relations in Prandtl co-ordinates. Both δ and R^{+*} are directly accessible from gross flow measurements.

The factors which represent the 'amount' of polymer *vis-à-vis* drag reduction are not obvious *a priori* but polymer concentration is evidently one such. Recent experiments concerning the effect of polymer concentration on drag reduction (Virk & Baher 1970) have indicated that for a given polymer, solvent and pipe the slope increment δ varies approximately as the square root of polymer concentration, i.e.

$$\delta \propto c^{\frac{1}{2}}. \tag{16}$$

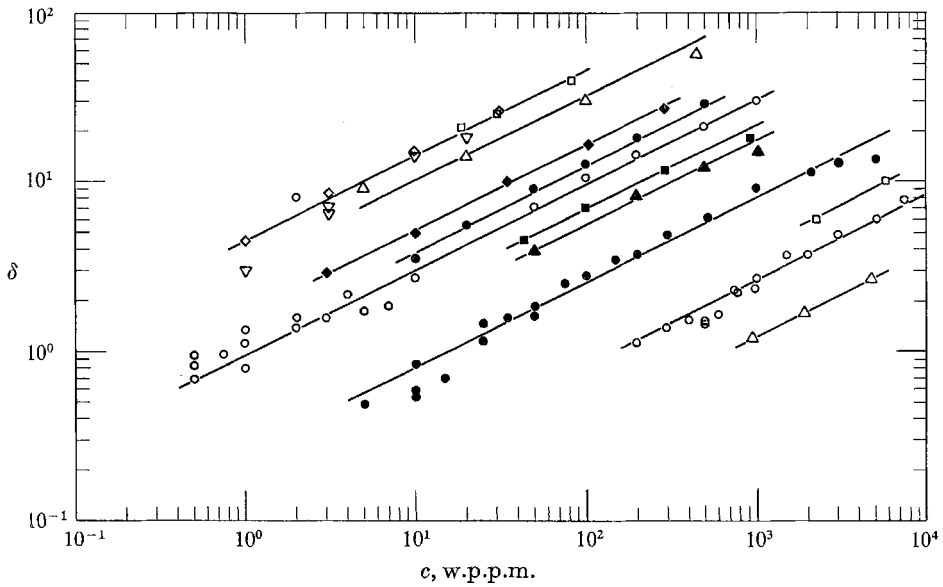

FIGURE 3. Effect of polymer concentration on slope increment for the polyethyleneoxide–water system. Corresponding experimental information is in table 4, symbols numbered as follows: ○, ●, 1–5; ▽, 6; □, ■, 7–9; ◇, ◆, 10, 11; △, ▲, 12–14. The highest molecular weight polymer used in a given pipe is denoted by hollow symbols, the next highest by solid symbols and so on alternately. Data for polymer N 80, only, have been shifted downward by a factor of 2 to prevent crowding.

However, the experiments from which (16) was inferred were of a preliminary nature and a more comprehensive collection of data concerning the relationship between δ and c is presented in figures 3 and 4. Figure 3 displays data obtained by the present author with the polyethyleneoxide–water system; corresponding experimental information is summarized in table 4. Each point on figure 3 represents a set of flow rate versus pressure drop data run with a given polymer solution and pipe: these were plotted in Prandtl co-ordinates and the slope, $[d(1/f^{\frac{1}{2}})/d\log_{10}(Ref^{\frac{1}{2}})] = 1{\cdot}626\ [dU^+_{\mathrm{av}}/d\ln R^+]$, obtained in the polymeric régime after onset but prior to the ultimate asymptote (if attained). For each pipe a

friction factor relation for solvent was also established experimentally, being very close to the Prandtl–Kármán law in all cases, and the slope increment δ was then the difference $(S_p - S_s)$ between polymer solution and solvent slopes in the same pipe. As can be seen from figure 3 and table 4, a range of concentrations were studied for each polymer and pipe, several molecular weight levels were investigated and various diameter pipes were used. All experiments were performed in

Entry	Pipe I.D. (cm)	Polymer designation	$[\eta]$ dl/g	M $\times 10^{-6}$	N $\times 10^{-4}$	Π $\times 10^{+6}$
1	0·292	N10	0·73	0·092	0·62	0·0081
2		N80	1·75	0·28	1·9	0·085
3		N750	3·38	0·63	4·3	0·24
4		N3000	3·90	0·76	5·2	0·34
5		W301	18·8	5·6	38	—
6	0·457	W301	18·0	5·2	35	2·93
7	0·846	N10	0·88	0·12	0·82	0·0145
8		N750	3·1	0·57	3·9	0·165
9		W301	18·5	5·5	37	3·4
10	0·945	W205	5·5	1·27	8·6	0·60
11		W301	18·0	5·2	35	3·3
12	3·21*	N10	0·66	0·080	0·54	0·0035
13		N3000	3·61	0·69	4·7	0·15
14		W301	20·1	6·1	41	2·5

Notes

* Recirculating system; molecular characterization refers to samples before use.

$[\eta]$, M, N, Π as noted below table 1.

All values of M are obtained from $[\eta]$ via the experimental correlation of Shin (1965) for the PEO–water system.

TABLE 4. Some drag reduction results for the polyethyleneoxide–distilled water system

once-through flow systems except for those with the 3·21 cm I.D. pipe which was part of a recirculating system. In figure 3: (1) The effect of polymer concentration on slope increment can be observed by following data for a given polymer and pipe. In all cases, covering concentration ranges of from $\frac{1}{2}$ to $3\frac{1}{2}$ decades, lines of slope $\frac{1}{2}$ apply within experimental error, upholding the square-root law (16). (2) The effect of polymer molecular weight can be noticed from sets of δ *vs.* c obtained with different homologues in a given pipe. While all homologues yield the same slope of $\frac{1}{2}$ in the chosen co-ordinates, the proportionality constant between δ and $c^{\frac{1}{2}}$ increases strongly with increasing molecular weight. (3) The effect of pipe diameter upon the δ *vs.* c relationship appears to be small. This conclusion is not readily apparent from figure 3 because the polymers employed in the various pipes differed somewhat in molecular weight which latter is itself an important variable. However, if values of δ at a given concentration (say 100 p.p.m.) are plotted against a molecular parameter (say intrinsic viscosity), results from all pipes from 0·292 to 0·945 cm I.D. arrange themselves on the same curve whereas data from the 3·21 cm I.D. pipe yield values of δ somewhat lower than the rest. It is believed that this latter is due to recirculation which causes polymer degradation and hence an *in situ* molecular weight lower (but by an unknown factor) than that quoted in table 4 for the original, undegraded, samples.

Some δ *vs.* c results derived from the data of other workers for various polymer-solvent systems are shown in figure 4 of which, for clarity, part (*a*) refers to aqueous and (*b*) to organic solvents; corresponding experimental information is summarized in table 5. On the whole the three features noted in connexion with figure 3 are also evident on figure 4 and in particular it can be seen that each set of

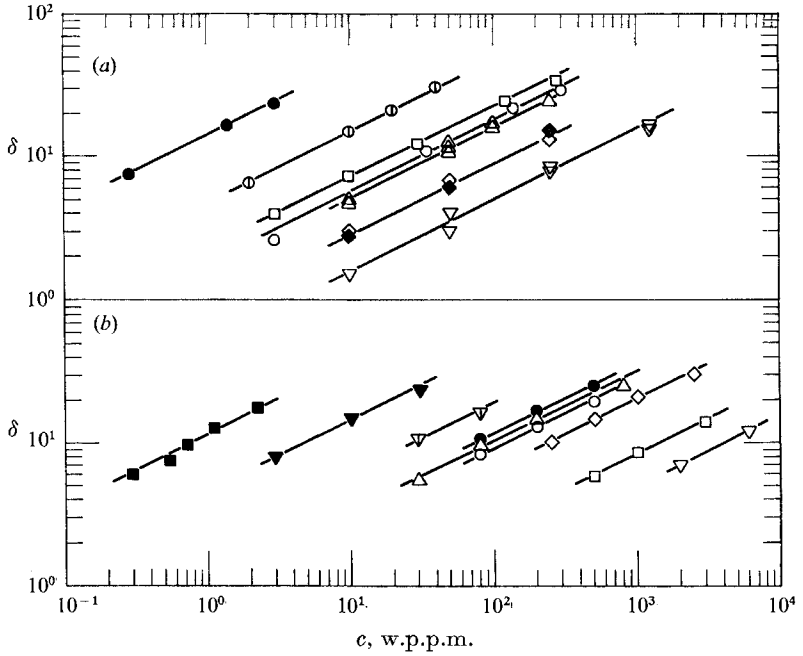

FIGURE 4. Effect of polymer concentration on slope increment for various polymer–solvent systems. Symbols are numbered to correspond to entries in table 5. (*a*) Aqueous solvents: △, 1; ▽, 2; ◇, 3; ◆, 4; ①, 5; □, 6; ●, 7; ○, 8. (*b*) Organic solvents: ■, 9; □, 10; ◇, 11; ●, 12; ○, 13; △, 14; ▼, 15; ▽, 16; ▽, 17. Data for entries 3 and 4 have been shifted downward by a factor of 2.

data is well represented by a line of slope $\frac{1}{2}$, further upholding (16). Attention should also be drawn to the more noteworthy aspects of individual entries. Whittsitt *et al.* (1968) cover a most impressive range of pipe diameters, 0·457 to 15·2 cm, and their data thus provide a striking illustration of the relatively weak influence of pipe diameter upon the δ *vs.* $c^{\frac{1}{2}}$ relationship. Pruitt, Rosen & Crawford's (1966) data for the same PEO polymer in two solvents, water and 0·6 molar K_2SO_4, are significant in that the expanded conformation of PEO in water, a good solvent, is markedly collapsed by addition of K_2SO_4, as reflected in this case by an intrinsic viscosity in 0·6 m K_2SO_4 about half that in water. This reduction in macromolecular coil size was found to alter the onset of drag reduction (same pipe) from $R^{+*} \sim 180$ in water to $R^{+*} \sim 280$ in 0·6 m K_2SO_4, but appears to have little effect upon the δ *vs.* $c^{\frac{1}{2}}$ relationship, as can be seen from figure 4(*a*). Shin's (1965) results were all obtained in turbulent Couette flow between concentric cylinders with the outer rotating and hence indicate that the square-root law applies also to flow configurations other than pipe flow. Finally,

the data of Liaw (1968) are noteworthy for the number of polymer-solvent systems studied, many of these for the first time ever with respect to drag reduction.

The experimental evidence presented in figures 3 and 4 indicates that the square-root form of (16) may be accepted with some confidence for drag reduction

Entry	Source	Pipe I.D. (cm)	Solvent	Polymer species	M $\times 10^{-6}$	N $\times 10^{-4}$	Π $\times 10^{+6}$
1	Whittsitt *et al.* (1968)	0·457, 1·06, 4·11, 15·2	Water	PAMH	(3)	9	0·9
2		0·457, 1·06, 4·11	Water	GGM	(0·22)*	0·09	0·075
3	Pruitt *et al.* (1966)	0·457	Water	PEO	0·83	5·7	0·51
4		0·457	0·6 m K_2SO_4	PEO	0·83	5·7	0·51
5	McNally (1968)	2·00	Water	PEO	3·4	24	2·75
6	Virk & Baher (1970)	0·945	Water	PAM	4·7	13	1·55
7	Shin (1965)	*Ro* 2·500 cm†	Water	PEO	4·7	32	4·9
8		*Ri* 2·283 cm†	Water	PEO	0·60	4·1	0·22
9		Gap 0·217 cm†	Cyclohexane	PIB	12	43	6·4
10	Rodriguez *et al.* (1967)	1·30	Cyclohexane	PIB	0·93	3·3	0·080
11	Toms (1948)	0·404	Chlorobenzene	PMMA	2·3	4·6	0·32
12	Liaw (1968)	0·272	Benzene	PEO	0·75	5·1	0·33
13		0·272	Benzene	PEO	0·48	3·3	0·20
14		0·272, 1·3	Toluene	PCIP	2·2	9·7	0·50
15		0·272	Toluene	PDMS	10·7	36	4·8
16		0·272	Toluene	PDMS	5·6	19	1·45
17		0·083	Toluene	PDMS	0·30	1·0	0·027

Notes

Polymer abbreviations and M, N, Π as noted below table 1.

Numbers in parenthesis are estimated, not experimental.

* Estimate for their sample kindly provided by Dr Whittsitt.

† Couette flow between concentric cylinders with outer rotating.

TABLE 5. Drag reduction results for various polymer–solvent systems

by dilute solutions of random-coiling polymers. Further, for a given polymer-solvent pair, the proportionality constant between δ and $c^{\frac{1}{2}}$ appears to be essentially independent of pipe diameter and might therefore be considered to characterize completely the effect of polymer concentration upon slope increment for solutions of that pair. The concentration range over which (16) applies is not yet fully defined. There appears to be no lower limit in that (16) holds as $c \to 0$ for as long as a slope difference can meaningfully be detected; however as $c \to \infty$, progressing from dilute to concentrated solutions, values of δ do eventually increase more slowly than $c^{\frac{1}{2}}$ (see e.g. the N 80 data in figure 3) with a non-dimensional concentration $c[\eta] \sim 0{\cdot}5$ tentatively representing this upper limit for application of (16). To summarize these findings, (16) is recast as an equation:

$$\Delta = \Pi(\mathcal{N}C/M)^{\frac{1}{2}}. \tag{17}$$

In (17), $\Delta\,(= \delta/S_s)$ is the slope increment normalized by solvent slope to render it independent of flow configuration, friction factor definition and the base to which logarithms of $Ref^{\frac{1}{2}}$ or R^+ are taken while $(\mathcal{N}C/M)$ is polymer concentration

in molecules per unit mass of solution, $\mathcal{N}$ being Avogadro's number, M molecular weight and C the conventional mass concentration in gm polymer/gm of solution (i.e. 10^{-6} times the concentration in w.p.p.m.). The proportionality constant, Π, thus represents a fractional slope change per macromolecule added and might therefore properly be termed an 'intrinsic' slope increment. Values of Π derived via (17) from figures 3 and 4 are listed in the final columns of both tables 4 and 5 and it will be noticed that the intrinsic slope increment varies widely from entry to entry indicating, as might be expected, that the polymeric entity ψ (or δ) depends also upon molecular parameters other than concentration.

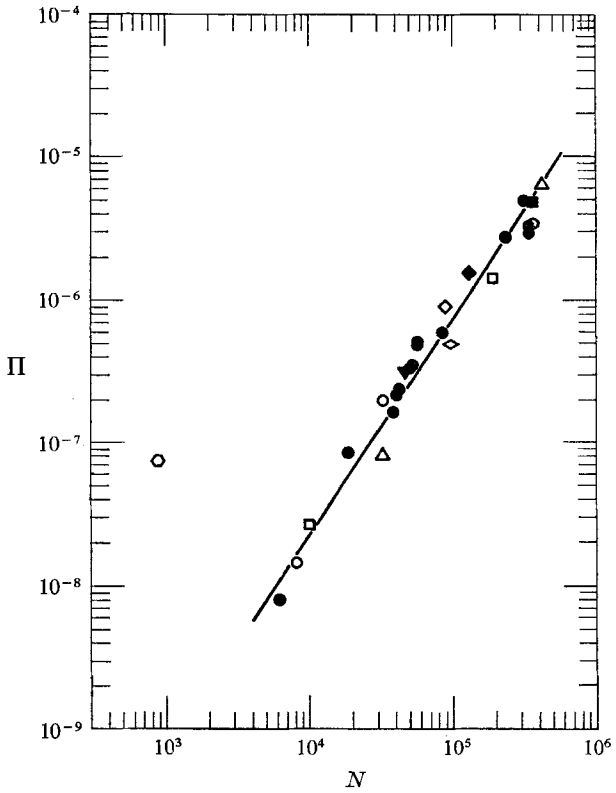

FIGURE 5. Relationship between intrinsic slope increment and number of backbone chain links for some linear random-coiling macromolecules. ⬭, GGM, water; ◇, PAM, water; ◈, PCIP, toluene; □, PDMS, toluene; ○, PEO, water, benzene, 0·6 m K_2SO_4; △, PIB, Cyclohexane; ▽, PMMA, chlorobenzene.

In seeking these latter, the intrinsic nature of Π entitles one to expect, at least initially, that it be related to some characteristic of the macromolecule itself. The single most important configurational parameter associated with the unique properties of macromolecules is the number of chain links, N, in the primary polymeric backbone; for linear (unbranched) macromolecules N is equal to the molecular weight divided by a constant factor, m, which is characteristic of the species and can be derived directly from the chemical structure of its repeating unit; e.g. $m = 14{\cdot}7$ for polyethyleneoxide. The number of backbone chain links

possessed by each of the polymers included in figures 3 and 4 are noted in the penultimate columns of tables 4 and 5. For these data the variation of intrinsic slope increment with backbone chain length is shown graphically in figure 5, a double logarithmic plot of Π *vs.* N. In this figure symbols are used to distinguish the various polymer species with the associated solvents indicated in the legend: the solid points (of whatever symbol) denote cases in which values of Π were obtained from polymer concentration ranges of a decade or more and values of N were based on positive polymer characterization while hollow points represent cases in which one or the other of these conditions was not fulfilled. Formally, the Π, N relationship should be sought for each species-solvent combination but perusal of figure 5 shows that, except for guar gum, *all* of the data lie on approximately the same curve, a straight line of slope $\sim \frac{3}{2}$ which implies a simple power law of the form

$$\Pi = KN^{\frac{3}{2}}. \tag{18}$$

Equation (18) with a proportionality constant $K = (2{\cdot}3 \pm 0{\cdot}8) \times 10^{-14}$ is indicated over the range $0{\cdot}5 \times 10^4 < N < 0{\cdot}5 \times 10^6$ by the solid line in figure 5. That all of the polymer species involved, which include most of the random-coiling polymers thus far studied in the drag reduction literature, should obey much the same Π *vs.* N relationship is mildly remarkable and establishes the number of backbone chain links as a relevant molecular parameter. However, the ± 30 % uncertainty in the above collective value of K admits to considerable variation on a scale finer than can presently be detected and the guar gum point yields a value $K \sim 280 \times 10^{-14}$ very distinctly different from the others so that it is advisable to consider K as characteristic, in general, of species-solvent pair of which the particular cases represented in figure 5 possess similar values.

The foregoing development concerning the polymeric 'amount' factor ψ postulated in connexion with elastic sublayer thickness can now be summarized. It was shown first that ψ was related to the difference δ between polymer solution and solvent slopes in Prandtl co-ordinates in the polymeric régime of drag reduction. From experimental data it was next demonstrated that for dilute solutions of random-coiling polymers this slope increment δ was proportional to the square root of polymer concentration. An intrinsic slope increment, Π, was then defined, (17), and shown to vary as the three-halves power of the number of backbone chain links, N, in the macromolecule. The proportionality constant, K, between Π and $N^{\frac{3}{2}}$ is nominally a function of polymer species-solvent combination but a single value approximately describes all of the present results for polymers other than guar gum. Combination of equations (15), (17) and (18) leads to the following final experimental relation

$$\psi = (\mathcal{N}C/M)^{\frac{1}{2}} N^{\frac{3}{2}} [KA_n/(A_m - A_n)], \tag{19}$$

where the square bracket is characteristic of a species-solvent pair (recall that A_m, A_n are the respective universal slopes of the semi-logarithmic ultimate and Newtonian mean velocity profiles).

Turning next to the factors concerning the 'excitation' of a macromolecule by the turbulent flow field, it will be recalled that these were embodied in the parameter R^{+*}, the value of R^+ at the onset of drag reduction. Onset, a striking

feature of the Toms phenomenon, has received considerable attention in the literature and since the available information has recently been summarized (Virk & Merrill 1969) the topic will only be taken up briefly here. Experimentally, the flow and polymeric parameters most relevant to onset appear to be, respectively, the onset wall shear stress T_w^* and the r.m.s. radius of gyration R_g of the

Polymer species	Solvent	Ω	R_g Range Å	Source
PDMS	Toluene	$0{\cdot}009 \pm 0{\cdot}003$	200–1500	Liaw (1968)
PIB	Cyclohexane, Benzene, Toluene	$0{\cdot}010 \pm 0{\cdot}002$	300–1100	Hershey & Zakin (1967); Rodriguez *et al.* (1967)
	Kerosene	$0{\cdot}010 \pm 0{\cdot}002$	500–1100	Ram, Finklestein & Elata (1967)
	Iranian crude oil	$0{\cdot}0027 \pm 0{\cdot}001$		
PAM	Water	$0{\cdot}0083 \pm 0{\cdot}001$	1500–4000	Virk & Baher (1970); Virk (1971)
PEO	Water	$0{\cdot}0065 \pm 0{\cdot}0015$	300–2500	Virk *et al.* (1967)
	Benzene	$0{\cdot}0075 \pm 0{\cdot}0025$	400–1700	Liaw (1968)

TABLE 6. Onset constants

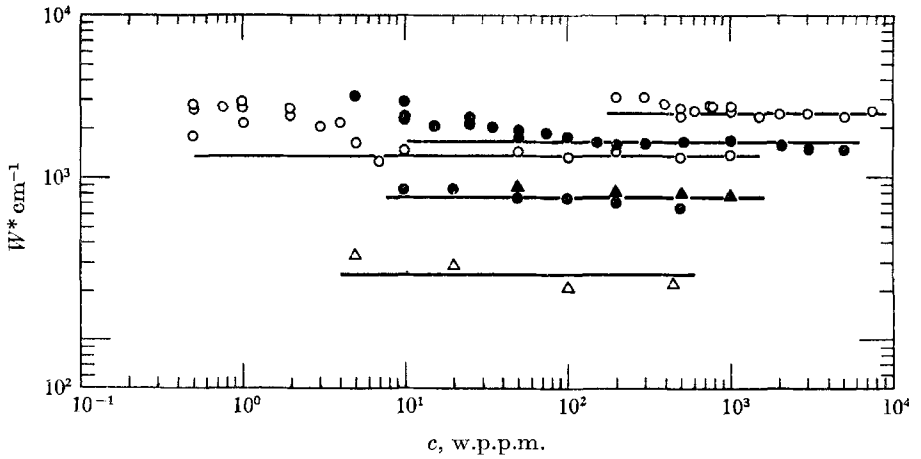

FIGURE 6. Onset wave-numbers corresponding to slope increment results for the PEO–water system as shown in figure 3. ○, 0·292 cm I.D. pipe; △, 3·21 cm I.D. pipe.

macromolecule in dilute solution. In terms of an onset wave-number, $W^* = u_\tau^*/\nu_s$, formed from T_w^* and solvent viscosity the observed relationship is of the form:

$$R_g W^* = \Omega, \tag{20}$$

where Ω is an empirical onset constant (dimensionless) characteristic of a polymer species-solvent combination and approximately independent of pipe diameter, polymer concentration and homologue molecular weight. Onset constants for

some cases of present interest are given in table 6 and the excitation parameter R^{+*} can be ascertained from these in an obvious way. It should be pointed out that previously, as in the derivation of (20), onset has been defined by a visual estimate of the point at which the polymer solution data depart from solvent. In the present work the experimental evaluation of δ, which requires fitting a straight line to best represent data for a given polymer solution in Prandtl co-ordinates, yields a corresponding onset point, defined by the intersection of the best-fit and solvent lines, that will differ from the previous if the data exhibit any curvature on the chosen co-ordinates. The magitude of such differences can be assessed from figure 6 wherein values of W^* corresponding to a portion of the PEO-water data displayed in figure 3 are plotted; it may be verified that these results are broadly in accord with the onset relation (20), the relatively weak influence of polymer concentration being especially evident. Similar results were obtained with all of the data presently analyzed and there thus appear to be no important differences between onset points associated with δ and those arrived at previously.

3. Theoretical

Because the macromolecules contained therein are capable of elastic deformation, particles of a dilute polymer solution can possess both mean and turbulent strain energies in addition to and analogous with the mean and turbulent kinetic energies normally associated with Newtonian fluid particles in a turbulent flow field. It is our belief that the basic polymer-turbulence interaction responsible for drag reduction involves the production of turbulent strain energy and that the elastic sublayer of our mean flow model physically represents the region wherein this additional entity affects the normal Newtonian energetic processes. If this basic premise is proper then the parameters that scale the elastic sublayer, and hence drag reduction, should arise from the turbulent strain energy and the object of the present section is to devise a theoretical expression for the latter in order to interpret the empirical results of the previous section.

The strain energy, S, per unit of a dilute polymer solution is the molecular concentration ($\mathcal{N}C/M$) times the strain energy per molecule, s_m. From the theory of rubber elasticity (Treolar 1958),

$$s_m = \tfrac{1}{2}\mathcal{k}T[(\langle L'^2\rangle/\langle L^2\rangle) - 1], \tag{21}$$

where $\mathcal{k}$ is Boltzmann's constant, T absolute temperature, $\langle L^2\rangle$ the unperturbed mean-square end-to-end distance of the macromolecule and $\langle L'^2\rangle$ the principal mean-square end-to-end distance when extended. For small deformations of perfectly flexible random-coiling macromolecules in a steady velocity gradient G, Peterlin (1963), using the dilute solution model of Zimm (1956), has shown theoretically that

$$[(\langle L'^2\rangle/\langle L^2\rangle) - 1] = 0{\cdot}136\beta^2, \tag{22}$$

where the non-dimensional parameter β is defined by

$$\beta = (M[\eta]\mu G/\mathcal{N}\mathcal{k}T) \tag{23}$$

with μ the solvent viscosity. A result identical to (22) save for the constant, 0·1 instead of 0·136, has also been derived by Cerf (1967). The only direct experimental measurements of macromolecular extension are due to Cottrell (1968) working with dilute polyisobutylene–decalin solutions in a laminar Couette flow; for small deformations the experimental results tend to agree with the form of (22) but yield a proportionality constant $\sim 0{\cdot}01$ an order of magnitude lower than theoretical. The latter disagreement is believed (Cottrell, Merrill & Smith 1969) due to the real polymer chain being less than perfectly flexible as assumed in theory and for this reason the universal proportionality constant 0·136 in (22) is best replaced by another, P, which is of order 10^{-2} as found experimentally and could also possibly depend upon chain structure. The strain energy in a steady one-dimensional flow is then given by

$$S = P\mathscr{k}T(\mathscr{N}C/M)\,(M[\eta]\mu/\mathscr{N}\mathscr{k}T)^2G^2, \tag{24}$$

with all numerical constants hereafter absorbed into P. In turbulent flow, wherein (24) directly represents the mean strain energy $\bar{S}$, the entity of interest is the mean-square turbulent strain energy s'. Now, the response of a macromolecule to an external stimulus requires the co-ordinated movement of various sets of its individual segments, termed 'modes', and in a turbulent flow the macromolecule will necessarily suffer stimulation by the entire spectrum of turbulence. Therefore s' can be thought of as being distributed over all modes of the macromolecule at all wave-numbers of the turbulent flow field and a typical spectral element of s' will thus contain the strain energy associated with, say, the jth mode of the macromolecule at the kth wave-number. The form of this s' element is obtained by analogy with (24) in which the $(M[\eta]\mu/\mathscr{N}\mathscr{k}T)$ term has dimensions of time and can hence be replaced by an element, τ_j, representing the contribution of the jth mode to the macromolecular relaxation time while G^2 is replaced by an element, $k^2E(k)\,dk$, of the mean-square turbulent strain rate (i.e. the dissipation spectrum) where $E(k)$ is the kinetic energy density at wave-number k. The turbulent strain energy density is thus of the form

$$F(k) = P\mathscr{k}T(\mathscr{N}C/M)\sum_{j=1}^{n}[\tau_j^2k^2E(k)], \tag{25}$$

where the summation extends over all n modes of the macromolecule and, by definition,

$$s' = \int_0^\infty F(k)\,dk. \tag{26}$$

Following Zimm (1956) the relaxation time τ_j is the product of a fundamental molecular time scale τ_0 and a dimensionless eigenvalue, $\rho_j(j,k)$, which depends upon the excitation of that mode by the flow field in question. One can therefore factor τ_0 out of each term of the summation in (25) whilst leaving the associated eigenvalue behind and it can further be shown that τ_0 is proportional to the original time group $(M[\eta]\mu/\mathscr{N}\mathscr{k}T)$ provided $[\eta]$ refers, as is normal, to steady flow with zero shear. With this one finally obtains for the local turbulent strain energy

$$s' = [P\mathscr{k}T(\mathscr{N}C/M)\,(M[\eta]\mu/\mathscr{N}\mathscr{k}T)^2]\left[\int_0^\infty \sum_{j=1}^{n}\rho_j(j,k)\,k^2E(k)\,dk\right]. \tag{27}$$

Of the two square brackets on the right-hand side of (27) it will be noticed that the first consists entirely of molecular parameters associated with a given polymer solution whereas the second involves only the excitation of an individual macromolecule by the turbulent flow field. This separation of variables is evidently analogous to that employed in the experimental analysis and a closer connexion might therefore be sought between the first bracket and the 'amount' factor on the one hand and the second bracket and the 'excitation' factor on the other.

The first square bracket on the right-hand side of (27) possesses dimensions of [length]^2 and hence its square root represents a fundamental length scale, $\mathscr{L}$, arising from and characteristic of a polymer solution in the present context. The $M[\eta]$ product which occurs inside the bracket can be replaced (Flory 1953) using

$$M[\eta] = \Phi\langle L^2\rangle^{\frac{3}{2}} = \Phi\langle Nb^2\rangle^{\frac{3}{2}}, \tag{28}$$

where $\Phi(= 2{\cdot}84 \times 10^{23})$ is Flory's universal constant, $\langle L^2\rangle$ the mean-square end-to-end distance, N the number of backbone chain links and b the effective bond length per chain link; the first equality in (28) expresses the $M[\eta]$ product as a hydrodynamic volume per macromolecule whereas the second equality implies the usual relation between $\langle L^2\rangle$ and N for Gaussian chains. The fundamental polymer solution length scale is thus

$$\mathscr{L} = (\mathscr{N}C/M)^{\frac{1}{2}} N^{\frac{3}{2}} b^3 \mu (P/\mathscr{k}T)^{\frac{1}{2}} (\Phi/\mathscr{N}). \tag{29}$$

The first two terms on the right-hand side of (29) also appear in (19) of the previous section and the matching exponents on each of these in the respective expressions indicate a linear relationship between the empirical entity ψ and the theoretical length scale $\mathscr{L}$. While the full physical significance of a linear ψ, $\mathscr{L}$ relationship remains to be examined (note that the proportionality constant between ψ and $\mathscr{L}$ must possess dimensions of inverse length since ψ is dimensionless), comparison of (29) with (19) further implies that the empirical constant K of (18) vary as the molecular group $[b^3\mu(P/\mathscr{k}T)^{\frac{1}{2}}]$ relating to the species-solvent combination. The present set of data is by no means adequate to test this implication by individual species and solvents but it leads to two interesting observations for the purposes of which effective bond lengths of all species have been included below table 1, solvent viscosities can readily be obtained (all the data refer to room temperature) and the factor P is assumed constant. Notice first that of the entries in figure 5, which differ very widely in chemical structure but yield much the same values of K, the polymer species all possess similar effective bond lengths, $b \sim 4$ Å, whereas the solvents all have similar viscosities, $0{\cdot}008 \pm 0{\cdot}002$ poise, so that $(b^3\mu)$ is of the same order in all cases. Secondly, in the guar gum–water system, which was a notable exception to the collective curve of figure 5, the solvent viscosity is typical of the others but the polymer species possesses a cellulosic skeleton with $b \sim 20$ Å compared with $b \sim 4$ Å for all of the others and the observed K ratio $(280/2{\cdot}3)$ is of the order of the b^3 ratio $(20/4)^3$. Both of the above qualitatively agree with the implied dependence of K upon molecular parameters and suggest that a modified proportionality constant $K' = (K/b^3\mu)$, physically associated with the dynamic chain deformation factor P, would ultimately prove most characteristic of species-solvent combination. It

might also be noted that the dependence of $\mathscr{L}$ upon temperature is entirely contained within the $[b^3\mu(P/\ell T)^{\frac{1}{2}}]$ group; from the known tendencies of b and μ to decrease with increasing temperature the same might be expected of ψ though there is yet no experimental evidence whatever in this regard.

A theoretical linkage between the integral in the second square bracket of the turbulent strain energy expression (27) and the empirical excitation parameter $\ln(R^+/R^{+*})$ has not as yet been established. However, two physical insights available from inspection are worth noting. First, the bracket in question is evidently the usual dissipation integral with all ordinates altered by a (dimensionless) summation that couples the macromolecule to the local flow field; for a given macromolecule therefore, the major contributions to the integral arise from the dissipative wave-numbers or, physically, the local production of turbulent strain energy occurs in the eddies responsible for the dissipation of turbulent kinetic energy. Secondly, for a Newtonian flow the highest turbulent strain rates occur at the edge of the viscous sublayer, $y^+ \sim 10$, which must therefore be the radial location of maximum s' prior to onset. Hence the value of the excitation integral at $y^+ \sim 10$ at the onset of drag reduction is characteristic of incipient polymer-turbulence interaction and this should subsequently provide a criterion for locating the outer edge of the elastic sublayer during drag reduction.

4. Discussion

4.1. *Comparison with previous work*

The present 'elastic sublayer' mean flow model merits comparison with three previous schemes: the 'effective slip' model (Oldroyd 1948), the 'thickened laminar sublayer' model (Elata *et al.* 1966, Meyer 1966) and a recent modification of the latter (Seyer & Metzner 1969).

The earliest conjecture concerning mean flow structure during drag reduction is due to Oldroyd (1948) who postulated an 'effective slip' caused by "anomalous behaviour in a thin layer near the tube wall" which "would have no effect on the velocity distribution in the turbulent region except to superpose upon it a uniform velocity in the direction of flow". This effective slip model amounts to a one-zone scheme wherein the velocity profile is parallel to but displaced upward from the semi-logarithmic Newtonian law of the wall and, from experiments conducted since, such a zone has indeed proved a characteristic feature of the mean flow structure at low drag reduction. When the drag reduction is low our model is dominated by its outermost zone (zone 3 in §2) and hence incorporates the effective slip model but no quantitative comparison can be made since the latter was not formally related to flow and polymeric parameters.

According to the thickened laminar sublayer model, originally proposed by Elata *et al.* (1966) and by Meyer (1966), the velocity profile consists of two zones—a turbulent core as in the effective slip model and a laminar sublayer extended to its intersection with the former and thereby thickened relative to Newtonian. Further the displacement of the core from the Newtonian wall law, i.e. the non-dimensional 'effective slip' or the increase in the wall constant B, was postulated to vary as the logarithm of friction velocity with a proportionality constant α

characteristic of the fluid. Evidently the thickened portion of the laminar sublayer in this scheme corresponds to the elastic sublayer of the present model and thus the essential conceptual difference lies in the velocity profiles respectively associated with these intermediate segments. However, at low drag reductions the outermost region tends to dominate each model (both of which so reduce to Oldroyd's effective slip model) and the friction factor relations derived therefrom become insensitive to the inner segment velocity profile provided that the net result, i.e. the effective slip, is properly specified. Under these circumstances it can be shown that the Elata–Meyer 'fluid property parameter' α differs from our slope increment δ only by numerical factors. In regard to evaluation of their parameter α from experiments, both the original authors found it to be approximately independent of pipe diameter (as postulated) but nothing was, or has since, been noted concerning the effect of polymeric parameters save for an indication by Elata *et al.* (1966) that α varied linearly with polymer concentration for their guar gum–water system. The latter conflicts with the present finding of a square-root, not linear, concentration dependence but the following reasons lead us to believe that this disagreement is not particularly serious: first, some earlier data (Elata & Tirosh 1965) by the same authors for the same system yield, amongst scatter, a variation of α as $c^{\frac{2}{3}}$ rather closer to our exponent; second, the data of Whittsitt *et al.* (1968), also for a guar gum–water system, are quite well described by our square-root relation as shown in figure 4 (*a*); and third, the $\alpha \propto c$ result was derived from experiments with a single polymer-solvent system over a limited concentration range whereas our $\delta \propto c^{\frac{1}{2}}$ relationship stems from a somewhat larger body of data. The differences between the original thickened laminar sublayer scheme and ours become more pronounced as drag reduction increases and in the limit the former formally tends to a laminar velocity profile and hence, erroneously, to Poiseuille's friction factor law whereas our scheme was derived from and transforms properly to the experimentally-observed maximum drag reduction asymptote. Physically, the effects of the polymer–turbulence interaction can be lumped in an anomalous wall region only so long as the outer flow dominates; with increasing drag reduction the region of interaction occupies a larger fraction of the flow and must therefore be accounted for. Our model attempts to do so, through an elastic sublayer wherein the mixing length represents the ultimate polymer–turbulence interaction, whereas the thickened laminar sublayer model, with no such additional information, is unable to.

The thickened laminar sublayer model has recently been modified by Seyer & Metzner (1969) who retained the basic two zone structure of the original but devised a different empirical function for the wall constant B such that the latter asymptotically approaches a maximum value $B \sim 30$ (compared with 5·5 for Newtonian) with increasing friction velocity. This significantly improves upon the high drag reduction behaviour of the original scheme in that the tendency to Poiseuille's law is eliminated but still differs from our model at asymptotic maximum drag reduction as illustrated by figure 7 wherein the experimental data of Seyer & Metzner are displayed against their own model, indicated by dashed lines, and the present, shown by solid lines. In figure 7 (*a*), $U^+ vs. \log y^+$, it may be seen that outside of the usual viscous sublayer, $0 < y^+ < 12$, the

asymptotic velocity profile in the Seyer–Metzner scheme consists of the thickened portion of the laminar sublayer $12 < y^+ < 40$ and a semi-logarithmic portion $40 < y^+ < R^+$ with Newtonian slope $A \sim 2{\cdot}5$ but asymptotic wall constant $B \sim 30$ whereas in our model this region $12 < y^+ < R^+$ consists entirely of the semi-logarithmic segment denoting the ultimate profile with slope $A \sim 11{\cdot}7$ and wall constant $B \sim -17$. The experimental data are rather better represented by our profile which is interesting but not over significant by itself because both model profiles are necessarily approximations. A more important difference is that at high R^+, the former leads to a friction factor asymptote which has the

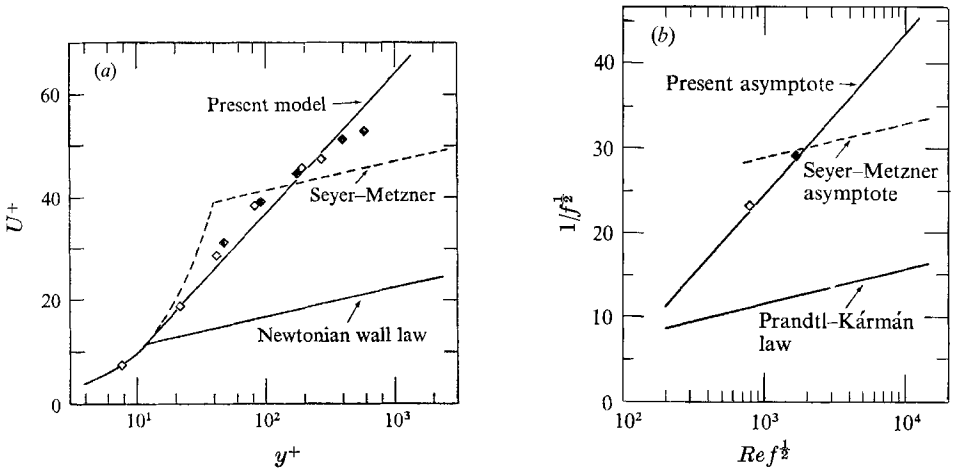

FIGURE 7. Comparison between present mean flow model and Seyer–Metzner (1969) scheme at asymptotic conditions; data of latter authors as in figure 2 & table 2. (*a*) Mean velocity profile. (*b*) Friction factor.

same slope as the Newtonian Prandtl–Kármán relation (1) but is displaced upwards in $1/f^{\frac{1}{2}}$ (by an amount $\sim (30 - 5{\cdot}5)/\sqrt{2}$) and this is not in accord with the experimental maximum drag reduction asymptote (2) implicit in our scheme, as shown in figure 7 (*b*), $1/f^{\frac{1}{2}}$ *vs.* log $Ref^{\frac{1}{2}}$. It may further be noticed on figure 7 (*b*) that the Seyer–Metzner asymptote intersects the experimental asymptote in the vicinity of the former's experimental data. This is the very region from which their empirical asymptotic value of B was derived by fitting the observed friction factors to the thickened laminar sublayer scheme; hence their asymptote agrees with experimental friction factors in the region of the fit but tends not to follow experimental results outside of this region. At low drag reduction the Seyer–Metzner scheme tends to the original thickened laminar sublayer model save that B is an empirical function of a non-dimensional time formed from the product of the relaxation time of the fluid and the wall shear rate. However, the fluid relaxation time requires separate experimental evaluation in each case and cannot be ascertained *a priori*; nor has any indication yet been given about its dependence upon molecular parameters so no comparisons can be made with the present work in this regard.

4.2. *Practical application*

The practical drag reduction problem is to predict a friction factor–Reynolds number relationship for the turbulent flow of an arbitrary but characterized polymer solution through a given pipe and it is therefore appropriate to summarize the present findings in this regard. In Prandtl co-ordinates, $1/f^{\frac{1}{2}}$ *vs.* $\log(Ref^{\frac{1}{2}})$, the friction factor relationship sought consists, in idealized general form, of three straight line segments corresponding to the flow régimes, (i) Newtonian, (ii) polymeric, (iii) maximum drag reduction, noted in the introduction. Of these, the asymptotic régimes (i) and (iii) are each independent of polymeric parameters and can be described by universal friction factor relationships respectively given by equations (1) and (2). The polymeric régime segment (ii), restricted to the region between (1) and (2), intersects the Newtonian segment (i) at the onset point $(Ref^{\frac{1}{2}})^*$ and possesses a slope exceeding that of the latter by a fractional amount Δ where both $(Ref^{\frac{1}{2}})^*$ and Δ depend upon the polymer solution as follows. From (20), the onset point is

$$(Ref^{\frac{1}{2}})^* = 2\sqrt{2\Omega}(R/R_g), \tag{30}$$

where R is pipe radius, R_g polymer radius of gyration in dilute solution and Ω a non-dimensional constant characteristic of the polymer species-solvent combination. Selected onset constants are listed in table 6; it is worth noting that a value $\Omega \sim 0{\cdot}008 \pm 0{\cdot}003$ encompasses practically all the onset results obtained thus far for random-coiling polymers in the common 'thin', $\nu \sim 0{\cdot}01$ cm^2/sec, solvents but there is essentially no information in solvents of significantly different viscosity. From (17), (18) the fractional slope increment is

$$\Delta = K(\mathcal{N}C/M)^{\frac{1}{2}}N^{\frac{3}{2}}, \tag{31}$$

where $\mathcal{N}$ is Avogadro's number $6{\cdot}02 \times 10^{23}$ and the polymeric parameters are C concentration as a weight fraction, M molecular weight, N number of backbone chain links and K a characteristic constant of the species-solvent combination. Data (see figure 5) indicate that for polymer species of carbon-carbon or similar types of skeletal structure in thin solvents $K \sim 2{\cdot}3 \times 10^{-14}$; there is also some indication that K (and hence Δ) is further proportional to the group $(b^3\mu)$ where b is effective bond length per chain link and μ solvent viscosity. In a friction factor relation obtained *a priori* as outlined above, the asymptotic segment (iii) will provide a reliable ($\pm 5\,\%$) indication of the maximum possible drag reduction but the polymeric régime segment (ii) presently permits only a crude (within, say, a factor of 2) estimate of the drag reduction to be expected therein. However, the remarks concerning calculation of the latter could prove useful for the practical problems of correlation and scale-up from limited experimental data.

The author is indebted to Professors F. R. Cottrell and H. S. Mickley of the Chemical Engineering Department, M.I.T., for their interest and assistance in the preparation of this paper.

REFERENCES

BEECH, D. R. & BOOTH, C. 1969 *J. Polym. Sci.* A2, **7**, 575.

CERF, R. 1967 *C. r. Acad. Sci.* (*Paris*), C**265**, 791.

COTTRELL, F. R. 1968 Sc.D. Thesis, M.I.T., Cambridge, Mass.

COTTRELL, F. R., MERRILL, E. W. & SMITH, K. A. 1969 *J. Polymer. Sci.* A2, **7**, 1415.

ELATA, C., LEHRER, J. & KAHANOVITZ, A. 1966 *Israel J. Technol.* **4**, 87.

ELATA, C. & TIROSH, J. 1965 *Israel J. Technol.* **3**, 1.

FABULA, A. G., LUMLEY, J. L. & TAYLOR, D. W. 1966 In *The Mechanics of Continua.* (Ed. S. Eskinazi). Academic.

FLORY, P. J. 1953 *Principles of Polymer Chemistry.* Cornell University Press.

FRUMAN, D. & SULMONT, P. 1968 *Rep. to Lab. d'Aërodynamique, Faculté des Sciences, Orsay.*

GILBERT, C. G. & RIPKEN, J. F. 1969 In *Viscous Drag Reduction.* (Ed. C. S. Wells). Plenum.

GOREN, Y. & NORBURY, J. F. 1967 *A.S.M.E. J. Basic Engng*, **89**, 814.

HERSHEY, H. C. & ZAKIN, J. L. 1967 *Chem. Engng Sci.* **22**, 1847.

HOYT, J. W. & FABULA, A. G. 1964 Paper to the *5th Symposium on Naval Hydrodynamics.*

KOLESKE, J. V. & KURATH, S. F. 1964 *J. Polym. Sci.* A, **2**, 4123.

KURATA, M. & STOCKMAYER, W. H. 1963 *Fortschr. Hochpolymer Forsh.* **3**, 192.

LAUFER, J. 1954 *NACA Rep.* no. 1174.

LIAW, G. C. 1968 Ph.D. Thesis, Univ. of Mo. at Rolla.

LUMLEY, J. L. 1967 *Appl. Mech. Rev.* **20**, 1139.

LUMLEY, J. L. 1969 *Ann. Rev. Fluid Mech.* **1**, 367.

MCNALLY, W. A. 1968 Ph.D. Thesis, Univ. of Rhode Island.

METZNER, A. B. & PARK, M. G. 1964 *J. Fluid Mech.* **20**, 291.

MEYER, W. A. 1966 *A.I.Ch.E. J.* **12**, 522.

OLDROYD, J. G. 1948 *Proc. 1st Int. Congress on Rheology*, V2, 130. North Holland.

PATTERSON, G. K. & FLOREZ, G. L. 1969 In *Viscous Drag Reduction.* (Ed. S. C. Wells). Plenum.

PETERLIN, A. 1963 *J. Chem. Phys.* **39**, 224.

PRUITT, G. T., ROSEN, B. & CRAWFORD, H. R. 1966 *Clearinghouse* AD 642441.

RAM, A., FINKLESTEIN, E. & ELATA, C. 1967 *Ind. Engng Chem. Proc. Des. Dev.* **6**, 309.

RODRIGUEZ, J. M., ZAKIN, J. L. & PATTERSON, G. K. 1967 *Soc. Petrol. Engng J.* **7**, 325.

ROUSE, P. E. 1953 *J. Chem. Phys.* **21**, 1272.

SAVINS, J. G. 1964 *Soc. Petrol. Engng J.* **4**, 203.

SEYER, F. A. & METZNER, A. B. 1969 *A.I.Ch.E. J.* **15**, 425.

SHIN, H. 1965 Sc.D. Thesis, M.I.T., Cambridge, Mass.

SPANGLER, J. G. 1969 In *Viscous Drag Reduction.* (Ed. C. S. Wells). Plenum.

TOMS, B. A. 1948 *Proc. 1st Int. Congress on Rheology*, V2, 135. North Holland.

TREOLAR, L. R. G. 1958 *The Physics of Rubber Elasticity*, 2nd ed. Clarendon.

VIRK, P. S. 1971 *J. Fluid Mech.* **45**, 225.

VIRK, P. S. & BAHER, H. 1970 *Chem. Engng Sci.* (to be published).

VIRK, P. S. & MERRILL, E. W. 1969 In *Viscous Drag Reduction.* (Ed. C. S. Wells). Plenum.

VIRK, P. S., MERRILL, E. W., MICKLEY, H. S., SMITH, K. A. & MOLLO-CHRISTENSEN, E. L. 1967 *J. Fluid Mech.* **30**, 305.

VIRK, P. S., MICKLEY, H. S. & SMITH, K. A. 1970 *ASME J. Appl. Mech.* **37**, 488.

WALSH, M. 1967 Ph.D. Thesis, Calif. Inst. Tech., Pasadena, Calif.

WELLS, C. S. 1965 *A.I.A.A. J.* **3**, 1800.

WELLS, C. S., HARKNESS, J. & MEYER, W. A. 1968 *A.I.A.A. J.* **6**, 250.

WHITTSITT, N. F., HARRINGTON, L. J. & CRAWFORD, H. R. 1968 *Clearinghouse AD* 677467.

WHITE, A. 1967 *Nature, Lond.* **216**, 994.

ZIMM, B. H. 1956 *J. Chem. Phys.* **24**, 264.